Int J Earth Sci (Geol Rundsch) (2005) 94: 301–316
DOI 10.1007/s00531-005-0471-6

ORIGINAL PAPER

F. G. Montesinos · J. Arnoso · R. Vieira

Using a genetic algorithm for 3-D inversion of gravity data in Fuerteventura (Canary Islands)

Received: 16 December 2003 / Accepted: 31 December 2004 / Published online: 9 March 2005

Abstract The use of genetic algorithms in geophysical inverse problems is a relatively recent development and offers many advantages in dealing with the non-linearity inherent in such applications. We have implemented a genetic algorithm to efficiently invert a set of gravity data. Employing several fixed density contrasts, this algorithm determines the geometry of the sources of the anomaly gravity field in a 3-D context. The genetic algorithms, based on Darwin's theory of evolution, seek the optimum solution from an initial population of models, working with a set of parameters by means of modifications in successive iterations or generations. This searching method traditionally consists of three operators (selection, crossover and mutation) acting on each generation, but we have added a further one, which smoothes the obtained models. In this way, we have designed an efficient inversion gravity method, confirmed by both a synthetic example and a real data set from the island of Fuerteventura. In the latter case, we identify crustal structures related to the origin and evolution of the island. The results show a clear correlation between the sources of gravity field in the model and the three volcanic complexes recognized in Fuerteventura by other geological studies.

Keywords Canary Islands · Gravity inversion · Genetic algorithm · Volcanism · Optimisation method

Introduction

Solving the inverse gravity problem entails determining the subsurface mass density distribution that accounts for the observed gravity anomaly field. The solution to this problem is non-unique (e.g. Al-Chalabi 1971) and is, moreover, limited because the data are restricted to a discrete set of inaccurate values. To deal with this issue, additional information about the model parameters (subsurface structure) and the data parameters (statistical properties of inexact data, e.g. Gaussian distribution) is taken into account in the inversion process.

Gravity inversion methods vary depending on the kind of model parameters selected, which may be the density (contrast) or geometrical parameters of the sources of the gravity field (anomalous bodies). On one hand, methods that consider the densities of the elements of a regular subsurface partition as unknowns (with non-discrete values) can use a linear approach (e.g. Camacho et al. 1997). In this case, the solution has a good fit to the observed data, but its geometrical properties are somewhat diffuse due to the smooth variation of the resulting distribution of density contrasts. On the other hand, methods that ascertain the geometrical properties of anomalous bodies with a fixed density contrast (e.g. René 1986; Barbosa et al. 1997; Camacho et al. 2000) correspond to a non-linear context and offer interesting results, limited only by the validity of the hypothesis made.

Generally, inversion methods look for analytical solutions by means of optimization techniques with linear approaches or iterative methods for linearizable problems. Unfortunately, linearized techniques greatly depend on the accuracy of the initial estimation of the model parameters (Rothman 1985). In fully non-linear treatments, local optimization techniques (steepest descendent, conjugate gradients, etc.) have traditionally proven inadequate due to their highly non-linear mathematical formulation, meaning local searches can, in some cases, be prone to being trapped in local minima. Although this is not very important for seismic velocity inversion and ray theory, it can be a significant issue in gravity inversion problem (e.g. Tarantola 1987). In these cases, the appropriate choice of a starting model is necessary in order to obtain satisfactory results. Also, these algorithms need information about the curvature in the solution space in order to establish the solution domain. Moreover, taking into account the inherent

F. G. Montesinos (✉) · J. Arnoso · R. Vieira
Instituto de Astronomía y Geodesia (CSIC-UCM),
Fac. CC. Matemáticas,
Av. Complutense, 28040 Madrid, Spain
E-mail: fuen@iagmat1.mat.ucm.es

ambiguity in the inversion of a potential field, these local methods are not always the most appropriate, and it is necessary to introduce particular constraints (Silva et al. 2001; Medeiros and Silva 1996; Scales and Tenorio 2001). Global optimization techniques by means of exploration methods (random or systematic) of the model space are considered good alternatives (Tarantola 1987). In this sense, optimization techniques based on Genetic Algorithms have opened up a new possibility for solving the inverse problem in a non-linear context in several areas of geophysics such as seismic applications (Boschetti et al. 1996; Billings et al. 1994; Sen and Stoffa 1995, etc.). In the study of the gravity inversion problem, Boschetti et al. (1997) used this optimization method, but only to detect the border between two bodies with different density contrasts.

Here, we present a Genetic Algorithm to resolve the inversion problem by determining the 3-D distribution of the subsurface sources of the gravity anomaly field corresponding to several a priori fixed density contrasts (positive and/or negative). Our gravity inversion method is tested with an artificial example and then applied, as real case, to the volcanic island of Fuerteventura (Canary Islands).

Gravity modelling plays an important role in the study of volcanic structures (e.g. Chandrasekhar et al. 2002; Rymer and Brown 1986). Thus, to provide insights into their internal structure and post-shield evolution, many gravity surveys have been undertaken on ocean island volcanoes, for example, in Hawaiiian chain (Kauahikaua et al. 2000; Zucca et al. 1982) or La Réunion (Rousset et al. 1989; Malengrau et al. 1999), Galápagos (Canales et al. 2002) and Azores (Camacho et al. 1997; Montesinos et al. 2003).

In Canarian archipelago, the geophysical and geodetic surveys which we have been carried out on several islands, give us a better understanding of their inner structure and evolution. This information is available from previous works on the islands of Gran Canaria (Camacho et al. 2000), Tenerife (e.g., Araña et al. 2000), Lanzarote (Camacho et al. 2001) and El Hierro (Montesinos et al. 2004) and from other geophysical studies (e.g. Ranero et al. 1995; Dañobeitia and Canales 2000; Carracedo 1996; MacFarlane and Ridley 1969; Bosshard and MacFarlane 1970). In Fuertevetura, we had performed previous studies using a regular grid of predicted gravity data (Montesinos 2002).

In this work, we apply our genetic algorithm to the observed gravity data on Fuerteventura, without resorting to an interpolated grid, which can alter or smooth the solution. Moreover, we complete the inversion model offshore using marine gravity data. Finally, we discuss the significance of the results.

The method

An inversion method is an optimization process that tries to find the model that best explains observed data and minimizes an error function. Among optimization techniques, Genetic Algorithms are search methods modelled on the evolutionary behaviour of biological systems, following Darwin's evolution principle. They are able to solve complex, non-linear optimization problems without the need for starting models or curvature information, simply by direct sampling of the solution space. They work by modifying a population of possible solutions, rather than a single solution, as is the case with most algorithms. Therefore, there is less risk of getting trapped in local minima because of inherent ambiguity of these problems, very far from the global minimum. Analogous to biological evolution, Genetic Algorithms treat these possible solutions as individuals who evolve by seeking to satisfy the optimization criterion. The individuals, who form the population, are represented with vectors (chromosomes) whose components are known as genes. In traditional Genetic Algorithms, each member of the population is represented in binary form. However, several authors show the usage of implementing a real code (e.g. Davis 1991). During successive generations, several operators act altering the chromosomes, while the process of natural selection ensures that the most successful individuals are selected and allowed to evolve. The success of each individual is of the result of a response to an error function. After several generations, the survivor which minimizes the error function is selected as the solution to the problem.

Gravity inversion using GA

We suggest the gravity inversion problem as an evolutionary process where individuals are possible models that represent the sources of the observed gravity anomaly field (anomalous bodies). We adopt the hypothesis that these structures are characterized by c prescribed mass density contrasts (d_q, $q = 1, \ldots, c$). Thus, the inversion problem consists of determining the geometry of the anomalous bodies corresponding to these density contrasts. In this case, our genetic algorithm (GA) is applied to a set of models (a population), making successive modifications in an iterative process, looking for a model that minimizes the discrepancy between the gravity field generated by the model and the observed gravity data (error function). To define the models, the subsurface volume close to the survey is divided into a fixed discrete 3-D partition of m prismatic elements. In this way, the anomalous sources are constructed assigning each prism one of the c prescribed density contrasts. The size of this subsurface partition coincides with the area where the gravity stations are distributed. The side of each prism is equal to the mean step between contiguous gravity stations. Each k-distribution of these density contrasts, for this partition, is a possible model $\mathbf{m}_k$ and therefore, a potential solution (good or bad) to the inverse problem. They are the individuals in the evolution process and they are represented by vectors (or chromosomes) of real numbers (genes),

$$\mathbf{m}_k = (\rho_1^k, \rho_2^k, \ldots, \rho_m^k)^{\mathrm{T}} \quad \text{with} \quad \rho_j^k = d_q \quad 1 \leqslant j \leqslant m; \;\; 1 \leqslant q \leqslant c,$$

where T indicates transpose.

Let us consider n gravity stations P_i (x_i, y_i, z_i), $i = 1,...,n$, not necessarily gridded, located on a rugged topography and with observed gravity anomaly values g_i. We assume that the observation uncertainties follow a Gaussian distribution, which can be expressed by a diagonal $(n \times n)$-matrix $\mathbf{E_{ss}}$, as deduced from the data analysis described in Sec. 4.2 (e.g. Camacho et al. 2000). The gravity attraction, A_{ij}, at the i-th station $P_i(x_i, y_i, z_i)$, due to the j-th prism, for unity density, is given by Pick et al. (1973)

$$A_{ij} = -G \Bigg[\Bigg[\Big[x \ln(y + (x^2 + y^2 + z^2)^{1/2}) + y \ln(x + (x^2 + y^2 + z^2)^{1/2}) + z \operatorname{arctg}(z(x^2 + y^2 + z^2)^{1/2} x^{-1} y^{-1}) \Big]_{u_1^j - x_i}^{u_2^j - x_i} \Bigg]_{v_1^j - y_i}^{v_2^j - y_i} \Bigg]_{w_1^j - z_i}^{w_2^j - z_i},$$

where G is the gravitation constant, the edges of the j-th prism are parallel to the reference axes, and the limiting coordinates for its volume are u_1^j, u_2^j for x-coordinate, v_1^j, v_2^j for y-coordinate, and w_1^j, w_2^j for z-coordinate. The matrix $\mathbf{A}$, with components A_{ij}, is the design matrix of the physical configuration of the problem and depends on the stations distribution and subsurface partition.

According to the direct problem, the gravity anomaly in the i-th station P_i, $i = 1,...\ n$, produced by the model $\mathbf{m}_k$ is

$$g_i^k = \sum_{j=1}^{m} A_{ij} \rho_j^k. \tag{1}$$

To obtain the solution of the gravity inversion problem, we define the error function that must be minimized, considering the discrepancy between the observed gravity, $\mathbf{g}_{\mathrm{obs}}$, and calculated data with the direct problem (1), weighted with the error matrix of the data $\mathbf{E_{ss}}$. In order to obtain more defined structural models, it is possible to include a regional tendency defined by one constant term, G_k, in each generation and dependent on the model $\mathbf{m}_k$ (Al-Chalabi 1971; Montesinos 2002). This is calculated by

$$G_k = \frac{\sum_{i=1}^{n} \left(g_i^{\mathrm{obs}} - g_i^k \right) e_{ii}}{\sum_{i=1}^{n} e_{ii}},$$

where e_{ii}, $i = 1,...,n$, are the diagonal elements of the $\mathbf{E_{ss}}$ matrix, which define the obtained error of gravity observation in the i-station.

To stabilize the inversion problem, we use the regularization technique of Tykhonov (Schwarz 1979), which includes a second member to minimize the quadratic expression of the model parameters. Thus, the selected error function for the GA is

$$F(\mathbf{m}_k) = (\mathbf{A}\mathbf{m}_k - \mathbf{g}_{\mathrm{obs}} - G_k\mathbf{u})^{\mathrm{T}} \mathbf{E}_{ss}^{-1} (\mathbf{A}\mathbf{m}_k - \mathbf{g}_{\mathrm{obs}} - G_k\mathbf{u}) + \beta\, \mathbf{m}_k^{\mathrm{T}} \mathbf{C}_M \mathbf{m}_k, \tag{2}$$

where $\mathbf{u}$ is unitary vector, β a regularization parameter and the $m \times m$ matrix $\mathbf{C}_{\mathrm{M}}$ describes the uncertainty of the model. This can be designed by a diagonal matrix with its elements defined by the inverse of the diagonal elements of $\mathbf{A}^{\mathrm{T}}\ \mathbf{E_{ss}}\ \mathbf{A}$. So, to each prism, we assign a value relative to the gravity attraction that it produces at the stations, defining in this way its uncertainty. Several techniques have been developed for estimating an appropriate regularization parameter β (e.g. Farquharson and Oldenburg 2004). We use a straightforward univariate search to find a value of β, which results in the first term of the error function similar to the standard deviations of the data noise. This criterion is widely used in geophysical inverse problems (e.g. Constable et al. 1987).

In each generation, this function is calculated by determining the fit of each individual and the probability of being selected for the next generation, as explained below.

The process starts with a population of np models, P(0), which can be generated randomly. However, to stay away from premature convergence to a non-suitable model, we select a starting population with all identical models, without information, where all the prisms have null density contrasts (empty models),

$$P(0) = \left\{ \mathbf{m}_1^0, \mathbf{m}_2^0, \ldots, \mathbf{m}_{np}^0 \right\} \quad \mathbf{m}_k^0 = (\overbrace{0, 0, \ldots, 0}^{m})^{\mathrm{T}} \quad k = 1, \ldots, np$$

The size of the population, invariant throughout the process, is believed to depend on the amount of unknowns and data, but the optimal relationship between the size of the population and the inversion parameters is still a matter of debate.

In the iterative procedure, the individuals of the population are evaluated and are chosen or not chosen (selection operator), to continue the evolutive process. Then, two genetic operators (mutation and cross) act on these selected models producing new individuals, which are also evaluated. If the operators produce ℓ new models, the selection operator chooses, from these np (old) $+\ell$ (new) models, the best np individuals that minimize the error function, and the iterative procedure is repeated.

Thus, from the initial population, the process starts with the evolutive cycle of evaluation/selection–mutation–cross and in the t-step, the population $P(t)$ will be formed by

$$P(t) = \left\{ \mathbf{m}_1^t, \mathbf{m}_2^t, ..., \mathbf{m}_{np}^t \right\} \quad \mathbf{m}_{.k}^t = (\rho_1^{tk}, \rho_2^{tk}, ..., \rho_m^{tk})^{\mathrm{T}}$$

where the density contrasts $\rho_j^{tk} \in \{d_1, d_2, \ldots d_c\}$, $j = 1,...,m$, $k = 1,...,np$. To simplify the notation, we will use $\{\mathbf{m}_1, \ldots, \mathbf{m}_{np}\}$ instead of $\{\mathbf{m}_1^t, \ldots, \mathbf{m}_{np}^t\}$

In each generation, the selection operator evaluates each individual with the error function (2), and it decides which ones are chosen for the other operators to act on them. From among the several selection options (Chu 1997; Goldberg 1989; Blickle and Thiele 1995, etc.), we have chosen an easy method that uses a roulette wheel with slots sized according to the fitness of the individuals (Michalewicz 1994; Baker 1987). To guarantee a faster convergence, the best individual always must be selected (De Jong 1975), and therefore, this operator only acts $np-1$ times. The roulette wheel is designed by (2), calculating the adjustment of the whole population, F_{T}:

$$F_T = \sum_{k=1}^{np} F(\mathbf{m}_k),$$

and a cumulative probability q_k, for each chromosome $\mathbf{m}_k$

$$q_k = \sum_{i=1}^{k} \frac{F_T - F(\mathbf{m}_i)}{\sum_{j=1}^{np} (F_T - F(\mathbf{m}_j))}.$$

The selection process is based on spinning the roulette wheel $np-1$ times, choosing a chromosome for a new population each time in the following way: to generate a random number $r \in [0, 1]$ and if $q_{k-1} < r \leq q_k$, we select $\mathbf{m}_k$, $k = 1, \ldots, np-1$.

Obviously, some chromosomes will be selected more than once (the best individuals will get more copies).

We apply the mutation and crossover operators to these selected individuals. The mutation operates on a gene-by-gene basis and provides random diversity in the population. It works according to a probability of mutation p_{m} and it is necessary to fix the number μ of mutated genes (i.e. the number of prisms in each model that can change its density contrast). To activate this operator, we assign each individual $\mathbf{m}_k$, $k = 1,\ldots,np$, a random number $r \in [0, 1]$. If $r > p_{\mathrm{m}}$; this model does not change any of their prisms. Otherwise, if $r \leq p_{\mathrm{m}}$, in this model, μ prisms will mutate, changing randomly its density contrast value among the c fixed density contrasts. As an innovation to traditional GA, the μ prisms, that must mutate, are selected according to its error e_j, $j = 1,\ldots,m$ (defined in the diagonal of the $\mathbf{C}_{\mathrm{M}}$ matrix of uncertainty of the model). The deeper and peripheral prisms (with a higher assigned accumulative error) must mutate more times because they have less influence on the error function. To do so, first, we calculate the accumulative error, e_j^a, to each j-prism in the q-model selected to mutate,

$$e_j^a = \sum_{i=1}^{j} \frac{e_i}{\sum_{k=1}^{m} e_k}.$$

Second, a random numbers $\in [0, 1]$ is generated. If $s < e_1^a$, then, ρ_1^q mutates, and if $e_{j-1}^a < s \leq e_j^a$, $(j = 2,\ldots,m)$ the gene ρ_j^q mutates. This process is repeated μ times for each individual selected to mutate.

The next operator consists of an exchange of genes between two individuals that undergo the crossover operation with probability p_{c} (e.g. Spears and De Jong 1991). The simplest way to cross is suggested by Michalewicz (1994). For each individual, $\mathbf{m}_i$, we generate a random number $r_{\mathrm{i}} \in [0,1]$. If $r_{\mathrm{i}} < p_{\mathrm{c}}$, then $\mathbf{m}_i$ is selected to cross. The selected models are coupled and for each pair of coupled chromosomes ($\mathbf{m}_i$, $\mathbf{m}_k$), where

$$\mathbf{m}_i = (\rho_1^i, \rho_2^i, \ldots, \rho_\ell^i, \ldots, \rho_m^i)^T \quad and$$
$$\mathbf{m}_k = (\rho_1^k, \rho_2^k, \ldots, \rho_\ell^k, \ldots, \rho_m^k)^T.$$

We generate a random integer number $\ell \in [1, m]$ the operator exchanging the genes acting between them from the position ℓ:

$$\mathbf{m}_i = (\rho_1^i, \rho_2^i, \ldots, \rho_\ell^k, \ldots, \rho_m^k)^{\mathrm{T}} \quad and$$
$$\mathbf{m}_k = (\rho_1^k, \rho_2^k, \ldots, \rho_\ell^i, \ldots, \rho_m^i)^{\mathrm{T}}.$$

These mutated and crossed models joined to unchanged ones are again evaluated and are subjected to selection/mutation/crossover operators repeating the evolutive process until a model that minimizes the error function is found, as described below.

The non-uniqueness of the gravity inversion could make some solutions to deviate to local minima. These deviations can be corrected by taking into account a priori information. Moreover, the solution obtained will depend on the reliability of the density contrasts chosen (positive and negative), which implies some uncertainty. High contrast values will produce an anomalous model with smaller and more compact structures than if we choose lower contrast values. The adjusted geometry for these anomalous bodies may appear too sharp and controlled by the selected density contrasts. To produce a model with a smoother geometry, we employ a smoothing technique equivalent to minimizing the total anomalous mass. This operator acts in each model by assigning each prism an averaged value of the density contrasts of the adjacent prisms. The smoothness works over the population with individuals near the final solution, when the error function becomes stable. Then, these smoothed new individuals are evaluated again. If the best model fits the observed gravity data successfully, according to the fixed limit (or it does not improve the previous models after several stages), the inversion ends, otherwise, the evolutive process is repeated.

In the inversion method, the density values can be invariant during the process (a dataset, with several positive and/or negative values). Another possibility consists of considering different density values according to how the process advances. Several authors have established the density–depth relationship with a simple mathematical law, for example, an exponential function (e.g. Cordell 1973). We can assume a similar density variation, but according to the number of times that the smoothness is applied and times the model has

consequently increased. Thus, we can fix the positive and negative maximum values, $\rho^{-}_{\max}$ and $\rho^{+}_{\max}$, and change these values during the smoothness technique for others according to the following exponential law:

$$\rho^{-}_{new}(k) = \rho^{-}_{\max} - \rho^{-}_{\max} \exp\left(\frac{-\zeta}{k}\right)$$

$$\rho^{+}_{new}(k) = \rho^{+}_{\max} - \rho^{+}_{\max} \exp\left(\frac{-\zeta}{k}\right)$$

where $k = 1 \ldots \zeta$ is the number of times the smoothness is applied.

The parameters used in this algorithm are empirically selected. Because of the amount of unknowns in the inversion process, it is not possible to consider a large population and, therefore, we select a small population size, but a high mutation rate forcing the introduction of very high diversity in the evolution. Reeves (1993) offers an algorithm to calculate the optimum size of the population for a fixed probability of success. Most of the authors (Reeves 1993; Grefenstette 1986; Michalewicz 1994, etc.) choose very low mutation rate values, about 0.01, because they usually work with few unknowns. Therefore, we suggest a high mutation rate value, between 0.2 and 0.6 (this value is increased if the amount of unknowns increases), with each individual mutating $\mu = 2$ genes. We select a crossover rate of about 0.6, which is close to the value recommended in the GA literature (Grefenstette 1986; Michalewicz 1994, etc.), because this operator has less influence than the mutation operator in the process. The change in one of these parameters does not significantly alter the results of the genetic algorithm, but does change its speed of convergence.

The program can always be worked on a personal computer (for example, Pentium V). First, we assay several solutions, with a model, with less resolution (for example, 2,000 prisms). In this case, the program can be run in just a few minutes (10′). When we have decided the different parameters, we can use a more refined model and then the program runs for more time.

Simulation test

To show the effectiveness and flexibility of the method, we use a synthetic example (Fig. 1). This simple test model is formed by a "T" body with a positive density contrast of 200 kg/m^3, similar to a "L" body with a negative density contrast of −200 kg/m^3 and W–E orientation. The volume of the "T" body is 32.5×10^9 m^3 and the mass centre is located at 2,500 m depth. The "L" body has a volume of 66×10^9 m^3 and an average depth of 2,750 m. Both bodies are located between 1,000 m and 5,000 m depth. The identification of the geometry of these bodies results in a non-trivial gravity inversion exercise. The gravity effect of the top of the "T" hides the existence of its deeper arm. Although it is not necessary, a planar regular grid (stepped 500 m and with an approximate side of 12×10^3 m) of 702 simulated stations with the same accuracy is adopted. The simulated gravity anomaly (Fig. 1) has a mean value of 0.750 mGal and a range of 11.290 mGal without adding any regional component.

The model is 7,000-m deep and 12,500×11,000-m^2 wide. It is divided into 5,844 prisms with 500 m sides (Fig. 2) and a distribution of uncertainty according to their distance to the observation sites. We apply the GA over these gravity data and an initial population of ten empty models (without any specific previous information) to ascertain the geometry of anomalous structures

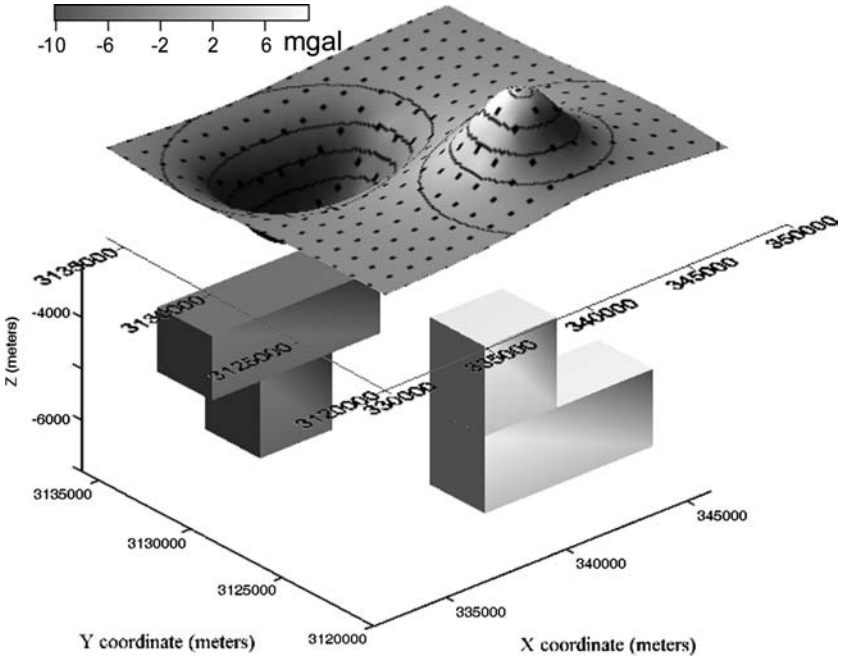

Fig. 1 Representation of the sources of the gravity anomaly field for the simulation test. Two bodies with geometry of "T" and "L", and with density contrasts of 200 and −200 kg/m^3, respectively, appear reaching depths of 6,000 and 7,000 m. On *top*, a gravity anomaly map corresponding to these sources with the distribution of gravity stations (*black points*). The contour interval is 2 mGal

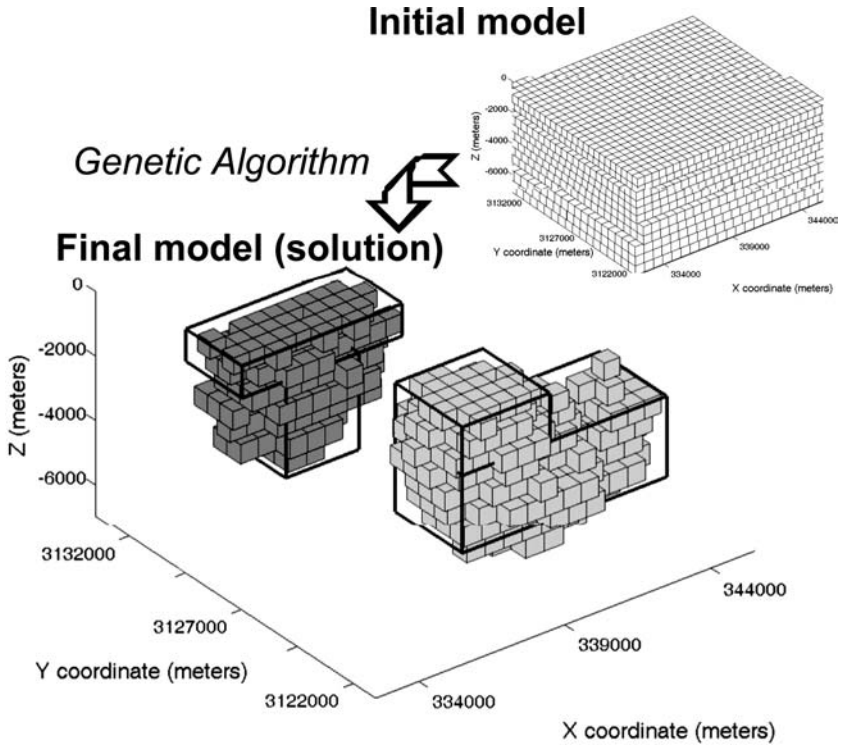

Fig. 2 Solution of the gravity inversion problem obtained by means of genetic algorithm for the simulation example "T–L" (shown with *thick black lines*). Prisms with a *light grey colour* correspond to a density contrast of 200 kg/m^3, and those with a *dark grey colour*, the ones of −200 kg/m^3. On *top*, the initial distribution of prisms is shown. These prisms, without assigned density contrast, constitute the individuals, which evolve reaching the solution (final model)

for a prescribed density contrast of 200 and −200 kg/m^3 throughout. Using other density contrasts, we would obtain a bigger model (with low density contrast) or a smaller model (with high density contrast). The algorithm of Reeves (1993) (applied in this case with 5,844 parameters) suggests a population size between 13 and 18 is necessary for successful exploration of the solution space. However, we select only ten individuals, increasing the traditional rate of mutation to 0.2. The smoothness operator acts several times during the evolutive process, giving as a result the best individuals in each stage, improving the previous fits. We stop the iterative process when the fit to the observed data is good ($<$ 0.1 mGal), and the iterative process is stable. The final solution—the best individual—(Fig. 2) fits the gravity data with a root mean square error of 0.115 mGal and an adjusted regional constant of 0.125 mGal. In this case, the smoothness operator acts after an average of 1,600 iterations and the selected final model is obtained in iteration number 192,984.

The inverted model is very similar to the synthetic one (Figs. 1, 2). Therefore, the additional condition of minimum anomalous mass, combined with the condition of minimum residual, gives rise to models that look for compact volumes for a level of fitness. So, the top of the "T" and "L" bodies are correctly identified although the deeper part of "T" is the worst recognized. Both the location and geometry of the "L" body are well recovered. The volume differences between the real and adjusted model are -5×10^9 m^3 for "T" and 0.03×10^9 m^3 for "L". The discrepancies between the gravity centre coordinates of the real and adjusted bodies are: $\Delta x^{T=-1}$ m, $\Delta y^T = -67$ m, $\Delta z^T = -280$ m and $\Delta x^L = -313$ m, $\Delta y^L = 22$ m, $\Delta z^L = -668$ m, respectively. According to the dimensions of the model, these differences are not significant, showing the efficiency of the method.

To show the applicability of this algorithm, we will now consider a real example on the basis of a gravity survey on the intra-plate volcanic island of Fuerteventura (Canary Archipelago).

Application to a real case: geological setting and previous works

Among the islands of the Canary Archipelago (between 27°38′ and 29°25′ latitude N and 13°20′ and 18°9′ longitude W) Lanzarote and Fuerteventura form the so-called the African group (Fig. 3). These islands represent the emergent part of the East Canary Ridge (ECR), which is a NNE–SSW linear volcanic structure off the Moroccan coast (Dañobeitia and Collette 1989). Although there is controversy about the genesis of the Canary Islands, it is now well accepted that the islands have worked as independent edifices (Schmincke 1982) located above an Upper Jurassic oceanic crust (Roest et al. 1992).

Fuerteventura exhibits the oldest subaerial volcanic rocks of the entire archipelago (Abdel Monem et al. 1971; Coello et al. 1992). The shield stage began 20.6 Ma ago, following the growth of a pre-Miocene seamount (Basal Complex) and ended in the mid-Miocene, after a very minor Quaternary post-erosional volcanism

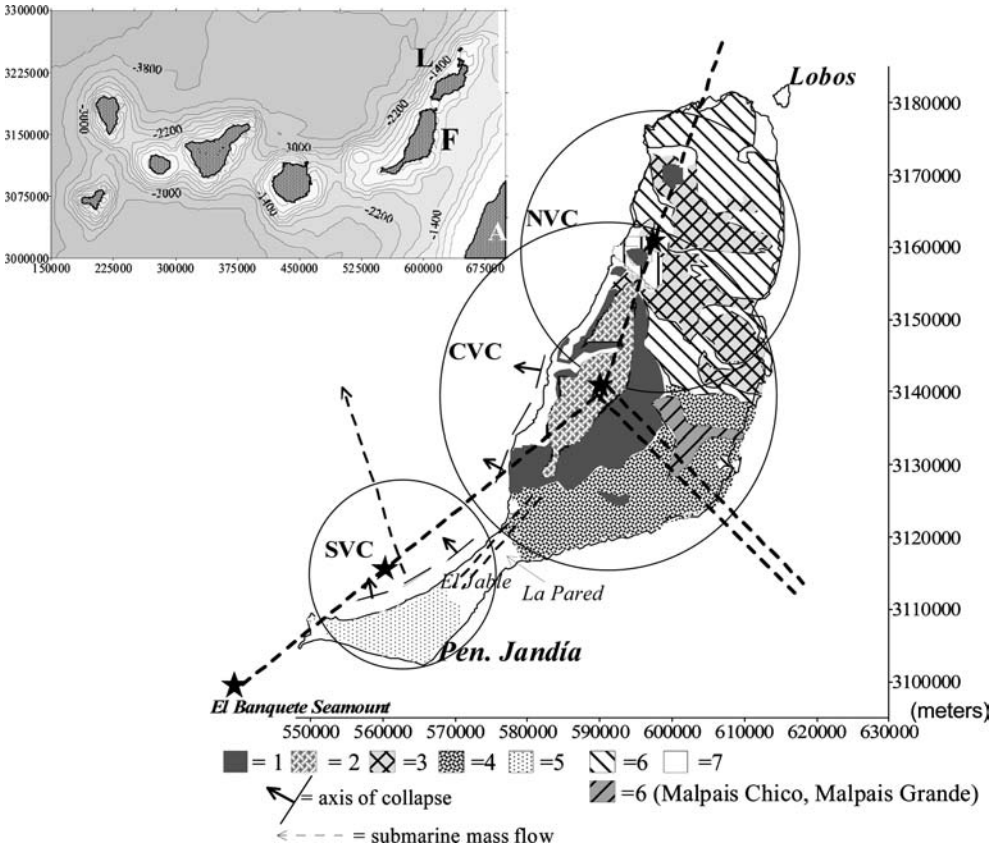

Fig. 3 Geological chart of Fuerteventura (adaptated from Ancochea et al. 1996; Stillman 1999): *1* Basal complex, *2* Basal complex zone of maximum dilation with general dyke orientation SSW-NNE, *3* North volcanic complex, *4* Central volcanic complex, *5* South volcanic complex, *6* Recent Series, *7* Sediments, *Star* Subaerial and submarine emission centres, *Dotted line* lineaments of volcanoes, *Double dotted line* Main directions of dyke intrusions; *Circles* approximate areas occupied by the volcanic complexes. Coordinates in UTM (meters). In the small figure, the location of Canary Islands and bathymetry (*F* Fuerteventura, *L* Lanzarote, *A* Africa)

(Carracedo 1996). At present day, there are only moderate volcanic highs. The rather subdued topography of the island rarely exceeds 400 m, reaching a maximum of 807 m only on the Jandía Peninsula (Fig. 4).

The Basal Complex (BC) has been interpreted in different ways, but most authors consider that it is the earlier substratum of the island, originated prior to the subaerial shield stage (e.g. Stillmann et al. 1975; Stillman 1999; Cantagrel et al. 1993). Ancochea et al. (1996) suggested that the BC represents the submarine growing stage of the volcanic complexes in this island and the hypabyssal roots (plutons and dykes) of their successive subaerial growing episodes. Socías and Mezcúa (1996) interpreted the basement of the islands of this archipelago as consisting of large tilted blocks, which have been differentially uplifted from the sea floor.

The upward continuation of the subaerial part of BC, the second major structural and petrological stage

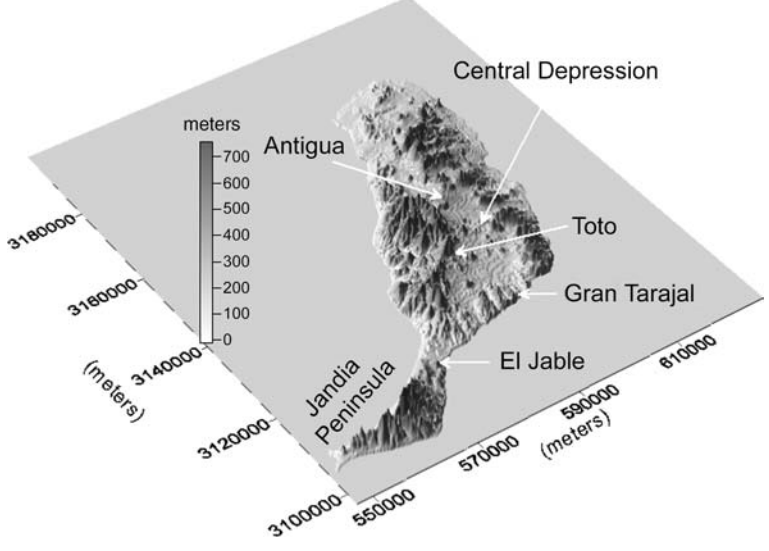

Fig. 4 Terrain model of Fuerteventura island with an orthographic SW–NE view. Highest altitudes are about 800 m at the peninsula of Jandía. In the central part of the island the area called the Central Depression can be observed. Several locations referred in the text are included. Coordinates in UTM (metres)

distinguished in Fuerteventura is the Subaerial Volcanic Series (SVS), where several different episodes have been recognized (Ancochea et al 1996; Cubas et al. 1992; Coello et al. 1992, etc.). The earliest (around 20–12 Ma) and most important is the Old Basaltic Series (OBS), which was followed by the recent series that continued until recent times (5– <0.1 Ma) (Coello et al. 1992). The recent series consists mainly of scattered pyroclastic cones and associated lava flows.

According to Ancochea et al. (1996), Fuerteventura is composed of three different adjacent volcanic complexes corresponding to the OBS: Southern (SVC), Central (CVC) and Northern (NVC). The geological map of the island showing the three complexes is displayed in Fig. 3. Each complex has its own prolonged history that might be longer than 10 Ma and partially independent. The volcanic complexes are deeply eroded and partially submerged and are along two main regional tectonic lineations. The SVC on the peninsula of Jandía is separated from CVC by a narrow, low and plain sector (El Jable). Dykes and the basalts are frequent in this complex.

The CVC is the oldest, and it extends from Antigua (Figs. 3, 4), where it overlaps the NVC, to El Jable. Three concentric semicircular areas are distinguished in this sector. The innermost and highest area is formed exclusively by the Basal Complex. It is surrounded by the Central Depression, a flat plain where altitudes do not exceed 100–200 m (Fig. 4), where BC and OBS rocks crop out. On the outermost area, only OBS materials are exposed. Dykes in the SE and SW areas of this complex are abundant (e.g. Feraud 1981). The remains of the NVC extend from the OBS northernmost exposures to the CVC. The OBS crops out mainly in the north and east, while the BC is exposed to the west and southwest. Both are partially overlain by younger volcanics (Recent Series) and sediments.

According to Ancochea et al. (1996), both the morphology and the dyke systems indicate the occurrence of large volcanoes, the centres of which are situated offshore in the case of SVC and onshore in the cases of CVC and NVC (Fig. 3). The bathymetry also attests to the occurrence of two more submarine edifices to the south of the island. Both seamounts show circular shapes that can be interpreted as corresponding to independent edifices of possibly similar characteristics.

With respect to the structural trends in Fuerteventura, the sheeted dyke net in the BC marks the main spreading trend and, therefore, the main regional trend. It is along this 15°N trend that the NVC and CVC centres are also aligned. There is a second N230°–N235° trend, parallel to main dyke intrusions in the El Jable area. The N135° dykes on southeastern Fuerteventura (Gran Tarajal) and their submarine prolongation could constitute the third arm of a possible junction (Figs. 3, 4). While, the first and second trends represent long standing regional tectonic alignments, the third one has been aborted.

Seismic studies have revealed that under the eastern islands, the crust displays a pattern of layer model but with pronounced structural differences between Lanzarote and Fuerteventura. Dañobeitia (1980), Banda et al. (1981) and Dañobeitia and Canales (2000), among others, characterized the crustal structure along these islands. These authors state that the crust beneath Fuerteventura is composed by an uppermost layer with a nearly constant thickness (4–5 km) and a mean velocity of 4 km/s, a 10–12 km thick mid-crustal layer with velocities of 6.5–6.7 km/s and a lower layer showing a velocity of 7.4 km/s, remarkably low for mantle velocity. This layer is interpreted as underplated material. Based on the refraction seismic profiles, Banda et al. (1981) suggested that the upper mantle beneath the island is anomalously hot, and that the crust is around 15-km thick. Dañobeitia and Canales (2000) reconsidered this interpretation and established a model with a smooth boundary between the lower crust and a diffuse crust-mantle boundary, slightly deepening towards the centre of the island. It reaches a maximum depth of 24–25 km, with a bulge amplitude of 4–5 km, possibly the result of flexure.

To use this information in the further gravity study it is necessary to assume some relationship between velocity, V_p, and density, ρ. Assuming the Carlson and Raskin's (1984) relationship for oceanic crust,

$$\rho(\mathrm{Mg\,m^{-3}}) = \frac{(3.81 \pm 0.02) - (5.99 \pm 0.11)}{V_p(\mathrm{km\,s^{-1}})}$$

this yields densities of 2,550 kg/m^3 for the first layer, 2,916–2,933 kg/m^3 for the crustal layer and 2,986 kg/m^3 for the lower layer. It is remarkable that because of the low velocity value in the third layer, the density values calculated for these two last layers are too similar. Unfortunately, the seismic experiment only involved a single transect of the island. So, these values, when extended to the whole island, offer some guidance, but can not be considered definitive in the interpretation of gravity models.

Dataset

Original topography and gravity data

To calculate the terrain correction of the gravity data, a digital terrain model was obtained for Fuerteventura and surrounding oceanic areas, by means of a dense regular digitalization of 1:50,000 topographic charts. Figure 4 shows an orthographic view of the resulting terrain model (57,915 data points). Because of the proximity of the island of Lanzarote, it is necessary to take into account its contribution to the terrain correction. To do so, we applied the terrain model calculated in previous work (Camacho et al. 2001). We completed the topographic maps with ETOPO5U (National Geophysical Data Center 1988) data where bathymetric values were scarce or unavailable (remote zone from the islands).

The gravity dataset comes from different sources. In 1993 and 1994, we observed a total of 325 stations on Fuerteventura with a LaCoste-Romberg gravimeter with digital electronic reading. These stations were nearly homogeneously distributed (separation between immediate stations of 1,500 m), and their coordinates were obtained by differential GPS (Fig. 5). We applied the usual corrections to these gravity data, such as drift, jumps and tides. To correct the tidal effect, we used the model calculated from the tidal gravity stations on the neighbouring island of Lanzarote (Arnoso 1996). The adjustment of the corrected observations produced residuals with a standard deviation 0.087 mGal ($1\ \text{mGal} = 10^{-3}\ \text{m/s}^2$).

To detect regional trend in the gravity data, we also used gravity data from Lanzarote and La Graciosa (Camacho et al. 2001) and marine gravity data. These marine data were: the free air anomaly map from US Geological Survey (USGS), with data collected from cruise in 1987 aboard the Starella Research Vessel (Folger et al. 1990) very near to the coast (about 30 km around the islands), and, for the zone farther from the islands (up to 75 km), data from the Defense Mapping Agency Aerospace Center (DMA), Geoscience Division, USA.

Data analysis and corrections applied

To detect errors in the topography of the gravity marine stations, we have compared the data with the available bathymetry of the zone. We also checked the quality of gravity values with a covariance analysis and a least-squares adjustment (Montesinos 2002; Moritz 1980). We used the covariance function calculated for the data to predict the gravity signal in the observation point by least-squares (Moritz 1980). The difference between this value and the observed gravity (residual) is used to detect the erroneous observations. If the residual is greater than two times the standard deviation, the observation is rejected. We applied the same corrections to the Bouguer anomaly map in order to establish the consistency and homogeneity of the different data sets, allowing a suitable covariance matrix corresponding to the inaccuracies for the gravity data to be obtained, which is useful in the following inversion process (e.g. Montesinos 2002; Camacho et al. 2000).

To calculate the Bouguer anomaly map, we used the 1980-normal gravity formula, and we determined the density value to apply the terrain correction, extended to 45 km away from each station, according to the regularity of the effect beyond this distance. Most gravity inversion studies use a standard density value to calculate this correction. The classic method of Nettleton (1939) calculates the terrain density by minimizing the correlation between the Bouguer anomaly and the topography. But this method is efficient only if the density of the formations is not related to the anomalous subsoil structure. In volcanic terrains, this correlation is generally predominant (e.g. Rymer and Brown 1986). For instance, the highest areas often correspond to the eruptive centres that involve density anomalies. To select a more suitable terrain density, we propose to choose the value that produces the smallest distortion of the gravity anomaly field. This value is the one that produces a minimum value of root mean square error, after applying the covariance analysis of the Bouguer anomaly and further least-squares prediction described above. Then, using this methodology, we considered a mean value of 2,500 kg/m^3 for the terrain masses density and a value of 1,027 kg/m^3 for sea water. The correlation factor between two datasets (topography vs. gravity corrected with a density value of 2,500 kg/m^3) is 0.35. This low value indicates that 2,500 kg/m^3 is a good approximation for the averaged terrain density. This terrain density is quite close to the value of 2,560 kg/m^3 that is obtained using Netleton's (1939) method, and it is also similar to the density value obtained for the first crustal layer (2,550 kg/m^3) from seismic data (Dañobeitia and Canales 2000).

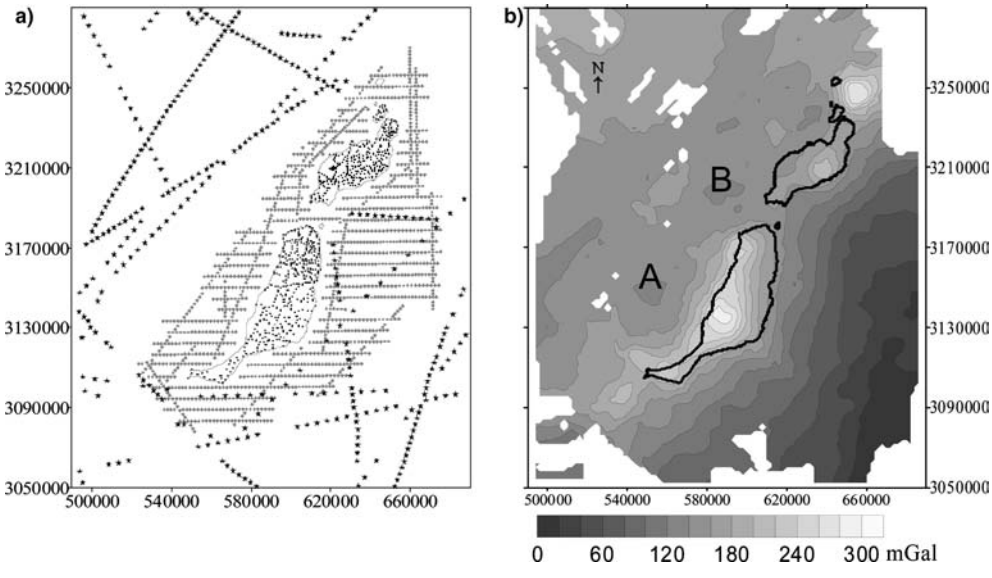

Fig. 5 **a** Distribution of gravity stations. *Black dots* Land gravity data (IAG); *Black stars* Marine gravity data from DMA; *light grey diamonds* Marine gravity data from Forguel et al. (1990) **b** Map of Bouguer gravimetric anomaly in Fuerteventura and Lanzarote calculated with a density of terrain correction of 2,500 kg/m^3. The contour interval is 20 mGal. UTM coordinates in metres. There are two minima (A, B), which could be related with the Jandía debris avalanche and East Canary Ridge landslide, respectively, identified in this zone by Krastel et al. (2001)

The covariance analysis and further least-squares prediction of the gravity signal over all the gravity stations has allowed bad tracks and/or points with large residuals (greater than two times standard deviation of data) to be removed. The process is repeated, applying the same removal criteria according to the new standard deviation until all data present small residuals. With this criteria and picking out marine stations with a minimum separation of 1,000 m near to Fuerteventura and 2,000 m away from the island, finally, we selected 168 and 1,289 points from DMA and USGS data banks respectively, 57 gravity data in Lanzarote, and the whole set of 325 stations in Fuerteventura, to calculate the Bouguer anomaly map of the region (Fig. 5). An inadequate terrain density would assign an excess of topographical anomalous masses as sources of the anomaly field, producing some fictitious local gravity anomalies. To reduce this problem, starting from the gravity data themselves, we have looked for a suitable terrain density that minimizes the gravity anomalies of topographic origin, keeping the anomalies due to the deep bodies. However, this is a typical approximation in gravity inversion studies and almost all authors use uniform density to perform the terrain correction.

In Fuerteventura, topographic features are rather subdued, so the terrain correction is less important than in other volcanic areas with rougher topography (for instance in Tenerife, Araña et al. 2000). A deficient terrain correction would be reflected in the inversion solution, but it would correspond to very local gravity anomalies and it would affect the fit between observed and calculated data only.

In this process we observe that the three different datasets from IAG, DMA and Forguel et al. (1990) are satisfactorily homogeneous (Fig. 5). They show a deviation of the non-correlated noise of 0.899 mGal for all gravity datasets and of 0.404 mGal if we consider only the land gravity data on Fuerteventura Island (Fig. 6). To obtain this result, we apply an analysis of covariance, determining an empirical covariance function and the corresponding analytical function, which let us filter the data using least-squares method (to subtract from the data a predicted signal with the identified function covariance). The final residual after applying iteratively the process corresponds to the data noise (uncorrelated part of the data) (Montesinos 2002). These values are conditioned by the accuracy of the (gravimetric and topographic) data and by the distance between stations and the horizontal gravity gradients (about 3 mGal/km) present in the area, deteriorating the final accuracy by the incorporation of marine data.

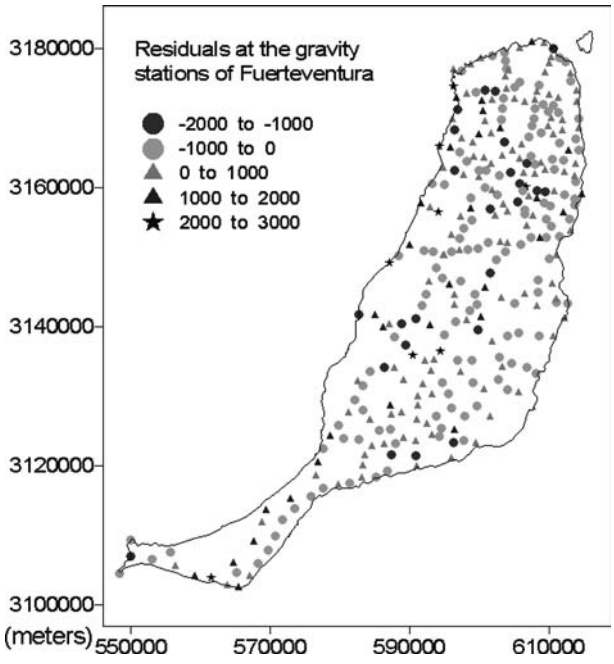

Fig. 6 Distribution of residuals (observed gravity data minus estimated gravity signal) corresponding to the covariance analysis of the 325 gravity data of Fuerteventura. These residuals can be considered as an estimation of the error or non-correlated noise of the data. The majority stations (257) have a residual of less than 1 mGal. They follow a normal distribution of mean 0 mGal and standard deviation 0.404 mGal. UTM coordinates in metres

Regional component of the gravity field and final gravity data

In a study of gravity field, the existence of a regional tendency in the data corresponds to a long-wavelength component, which could mask the effects of the local structures of interest in the investigation. Therefore, this regional component must be identified and removed from the gravity data. The resulting Bouguer anomaly map of the eastern-most Canary Islands (Fig. 5) shows a regional tendency that is possible to identify.

To detect a regional tendency in the gravity anomalies, it is necessary to work over a wider zone. Thus, we use the whole dataset considered in the previous process, identifying it through a polynomial fit by means of robust statistic (Beltrao et al. 1991). A polynomial surface of degree four is empirically selected. A lower degree does not reveal information, and a higher value does not modify it significantly.

This regional component (Fig. 7) is characterized by a stronger gradient between the islands and the neighbouring African coast, with respect to the plateau west from Fuerteventura and Lanzarote. These features can be related with the change in the crustal thickness and with the proximity of the continental margin. It also shows the same tendency as the flexure of the Moho, caused by the topography load calculated by Dañobeitia and Canales (1994), which reflects the maximum influence of the continent.

After removal of the regional trend from the Bouguer anomaly map, we picked out 660 data corresponding to the Fuerteventura Island and to the offshore zone (up to 20 km) (Fig. 7). This residual gravity map is characterized by positive anomalies, typical in basaltic volcanism (Rymer and Brown 1986), as in the case of Canary

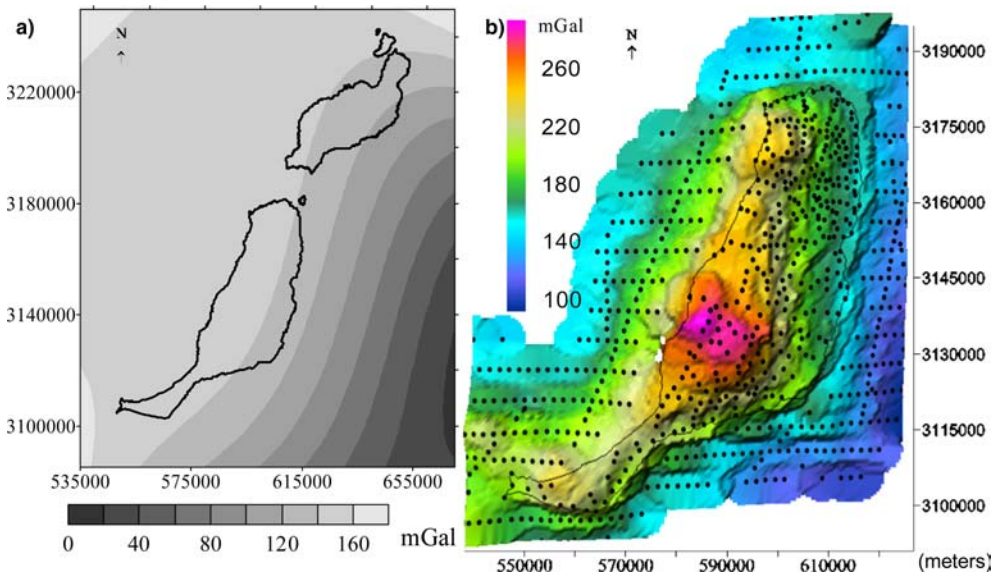

Fig. 7 **a** Regional component of the gravity field for the islands of Fuerteventura and Lanzarote calculated bay means of a polynomial fit. **b** A detailed 3-D view of the residual gravity map for Fuerteventura used in the inversion process. There is a main maximum, which almost occupies the centre of island where the Basal Complex is evident on surface. The final gravity station distribution used in the inversion process is overprinted. UTM coordinates in metres

Islands (e.g. Araña et al. 2000; Camacho et al. 2001; MacFarlane and Ridley 1969; Bosshard and MacFarlane 1970).

Results

Inversion procedure and parameters

To apply the proposed method of gravity inversion, we consider a subsurface volume partition with 16,707 parallelepipedic blocks of sides ranging from 1,600 m (up blocks) to 3,300 m (down blocks) and from 1,500 m to 25,000 m of depth. After several attempts, we selected the values of density contrast ranging between −300 kg/m^3 and 400 kg/m^3, with an exponential law of variation of the contrasts. These values are closer to the maximum differences among the mean densities calculated from seismic results and they are similar to those obtained for the gravity inversion on the island of Lanzarote (Camacho et al. 2001). The aim of selecting these density values is to obtain structural models in coherence with the geologic information, with compact volumes associated to the anomalous bodies. The selection of other higher values would produce similar models, but with more compact volumes.

In the case of this gravity study, the genetic parameters chosen are 0.6 as crossover probability, 0.3 as mutation probability, two genes mutate in each individual, the best individual is repeated two times in each generation, 0.1 as Tychonov parameter, 1.1 smoothness parameter and a population with 14 individuals, without initial distribution of density contrasts.

The final model

The genetic algorithm, with the parameters detailed above, is applied to the final gravity data obtained for Fuerteventura. Then, through the evolutive process, the smoothness operator acts several times, giving as a result the best individuals in each stage. When the best individual fits the observed data with a standard deviation of nearly 0.8 mGal (two times the error detected in the covariance analysis of the data), the smoothness operator starts to act, and the generation begins. In this case, the smoothness operator acts after an average of 61,300 iterations, and the final model is selected after 429,114 iterations. The value of the calculated constant, G_k, is used only to obtain more significant structures, it is not directly interpretable. Finally, our best solution is the model with a distribution of the sources of the gravity anomaly field, which provides the best fit to the observed gravity field and corresponds to plausible crustal structures, according to the geological and tectonic information. The final residual of the adjustment of observed anomalies by the gravity anomalies produced by the selected model follows a Normal distribution of mean 0.062 mGal and standard deviation 1.034 mGal (Fig. 8). So, the fit obtained for the observed gravity values is not far from the accuracy of the data obtained by means of the former covariance analysis (0.899 mGal). The majority of the gravity stations have a low residual value (less than 1 mGal), and they are homogeneously distributed (Fig. 8). Therefore, all the zones of the selected model have similar plausibility as solutions to the inverse problem. The density distribution at different depth levels is shown in Fig. 9.

Discussion

The gravity anomaly map (Fig. 5) points out much interesting information, such as the existence of a strong gradient between the islands and the African continent, a main maximum of gravity in the centre of each island and several smaller anomalies offshore. Krastel et al. (2001) identified several submarine landslides around the

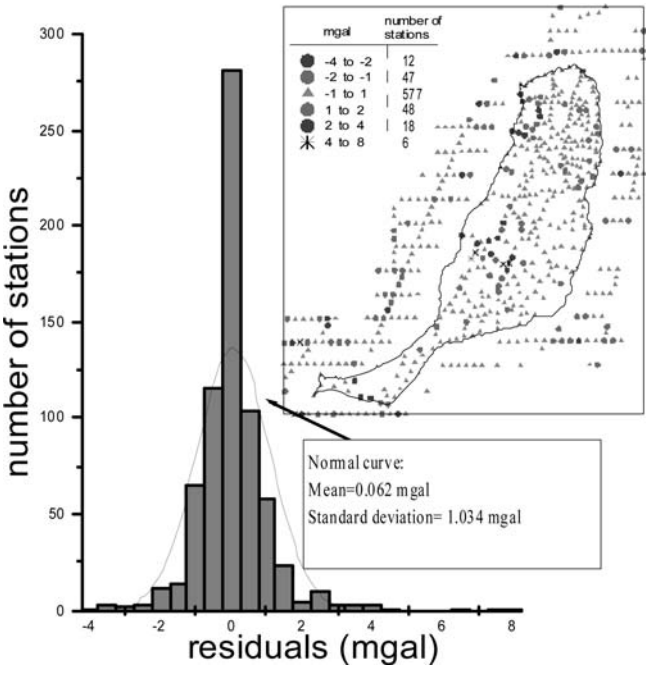

Fig. 8 Distribution of residuals corresponding to the inversion process for the gravity stations. In the table, we include the number of stations with the same residual level. The majority stations (577) have a residual of less than 1 mGal. On the island, those stations with the highest residuals correspond to locations with complicated topographic corrections. The histogram is adjusted by a Normal curve with mean 0.062 mGal and a standard deviation of 1,034 mGal, close to the precision value calculated for the data

Canary Islands. Their data also document giant landslides off the coast of the older eastern islands and suggest that a speckled backscatter pattern more than 35 km northwest of the peninsula of Jandía is caused by deposits from a debris avalanche, the so-called the Jandía debris avalanche. For these authors, the source area of this avalanche remains unclear, but a submarine origin is favoured. Moreover, they describe the deposits of a submarine mass-wasting event offshore in the gap between the islands of Lanzarote and Fuerteventura as consisting of two slumps and a debris flow. The minimum gravity anomalies which appear offshore to the west (in Fig. 5: A, B) could be related to these two submarine landslides around Fuerteventura and Lanzarote.

Our genetic algorithm highlights certain interesting features in the model of distribution of the density contrasts obtained (Fig. 9). However, it should be mentioned that the interpretation does not take into account horizontal stratification undetectable with the gravity inversion. It would be possible to add this information later from seismic results (Dañobeitia and Canales 2000).

In general, the various anomalous structures (contrasting in density with their surrounding) identified in the model can be associated with the three volcanic complexes and with the main tectonic features pointed out by Ancochea et al. (1996) for Fuerteventura (Figs. 3, 9). Among the structures with high density, which are predominant in the model, three main blocks can be pointed out along the island. They are continuously present from the shallow to the deeper levels of the model and appear aligned according to SW–NE trend, parallel to the African coastline. Their geometry is almost regular, and they present nearly circular edges. These three main blocks, with high densities in the deeper sections, can be associated with the original structure of the island. They are indicative of the lithospheric buildings of oceanic basement which formed the three volcanic complexes (Central, Northern and Southern). In the model, they appear to independent of each other, and this agrees with the theory that each complex was constructed in several different phases, in cycles of activity separated by tectonic stages.

The most important (largest and deepest) body is the central one, located in the zone where the BC is spectacularly exposed at the surface. Thus, this body is clear evidence supporting the hypothesis of an emplacement of mafic cumulates at the base of the crust in the eastern Canary Islands that produced crustal thickening beneath the OBS (Dañobeitia and Canales 2000). This anomalous body, associated with BC, is located in deeper sections, reaching a depth of over 25 km (Fig. 9). Hence, its characteristics are in agreement with the study of Dañobeitia and Canales (2000) about the crustal structure of this island and corroborate their results. These studies report that the boundary between the lower crust and Moho is deepest towards the centre of Fuerteventura and reaches a maximum depth of 24–25 km.

In the shallowest sections, this central body comprises several differentiated structures. The explanation could be that the main body began forming in the early stages and continued during several phases, giving rise to an heterogeneous association of materials, unique in the archipelago (Stillman 1999). Thus, there is a good relation between these shallower structures and the three concentric semicircular areas, which Ancochea et al. (1996) identified in the CVC (Figs. 3, 9): BC, Central Depression and Miocene lavas. The innermost and highest area near the coast formed by the BC, is associated in the model with a high density body. Moving westaward, the next structure in the model is another high-density body elongated in a NE–SW direction in the Central Depression zone. This body, related to the former in its deeper sections, was formed by the deposits in this depression covering and largely obscuring the eroded surfaces of both the BC and the OBS subcrop (Stillman 1999). The border of this second area, as pointed out by Ancochea et al. (1996), coincides with the border of this central body at shallower sections of the model. Finally, in the outer area of this complex, where these authors report the presence of OBS materials and superimposed Recent Series, there is only one remarkable body with negative density contrast in the area of Malpaís Chico and Malpaís Grande (Figs. 3, 9). Here, the Recent Series consist mainly of scattered pyroclastic cones and associated lava flows and, therefore,

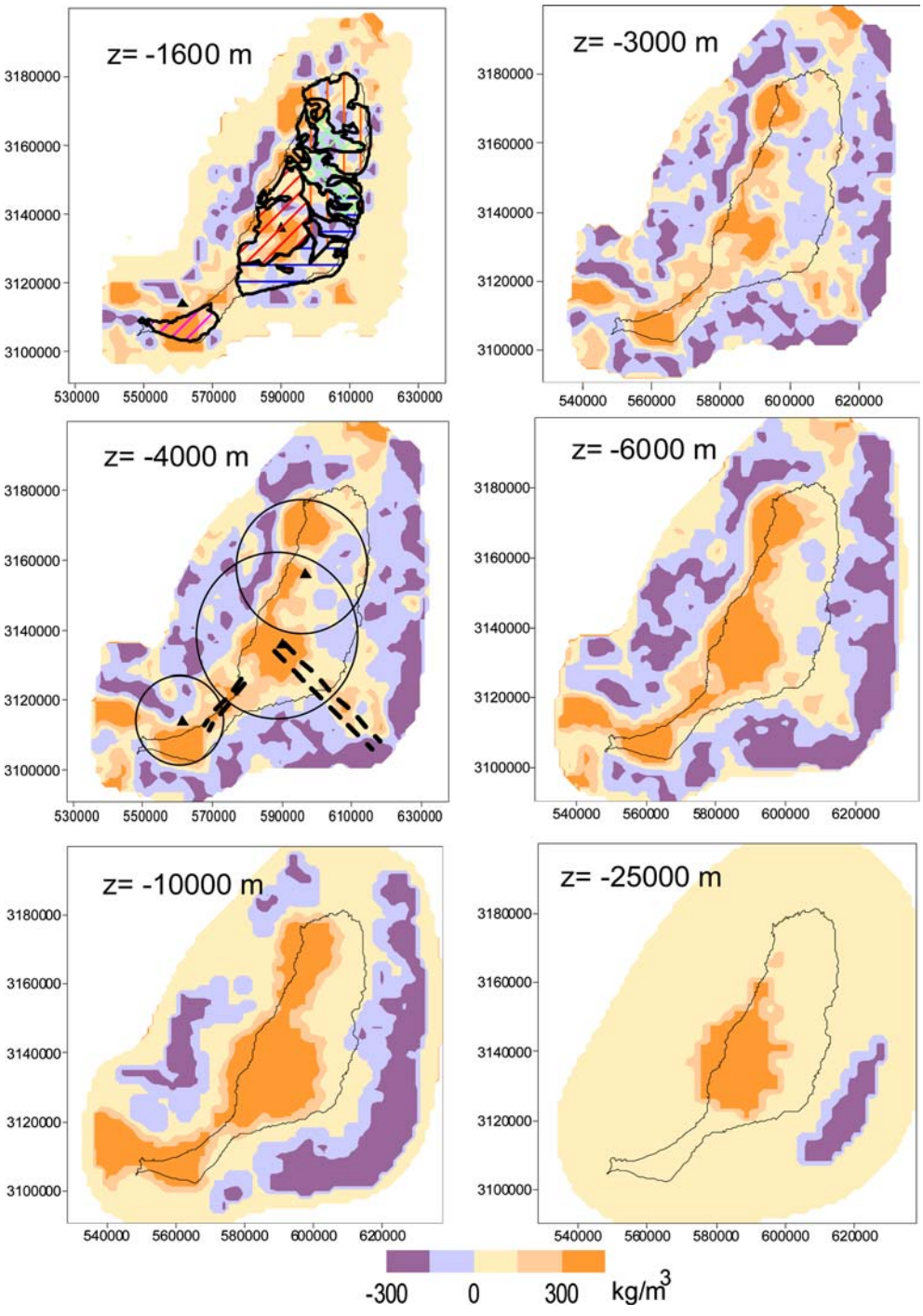

Fig. 9 Adjusted model of anomalous density contrast obtained by means of 3-D gravity inversion. Several horizontal sections, from 1,600 m to 25,000 m in depth, are shown. The quite regular geometry of the positive density contrast bodies is *highlighted*. In the shallowest section, the geological scheme of the island (Fig. 3) is pointed out. The concordance among different geological units and the bodies identified in the model is clear. In the section of 4,000 m depth, the areas occupied by the three volcanic complexes (Fig. 3) and the main trend of dyke intrusions are indicated

structures like those in the model, with low density, are congruent.

A possible eruptive centre of this complex pointed out by Ancochea et al. (1996) near Toto (Figs. 3, 4, 9) coincides with the centre of this main structure in the deep sections. In the shallowest sections of the model, this eruptive centre is placed between the two high density bodies identified and near a small body with negative density contrast. But this low density body appears related more with the structures linked to Malpaís Chico, where recent series volcanism took place, than with the main body of the model. Therefore, in the latter case, the existence of a volcanic construct with a cone centred near Toto and palaeocontours near coastlines can only be inferred, from this model, by looking at the general structure of this main central body.

In this area, various high-density bodies can be aligned with an approximate elongation in the direction of the southeastern coast, following a 135° N structural trend and the main dykes system, and with another elongation to the south–west following the other main

intrusion direction (Fig. 9). Moreover, the massive presence of dykes in the southeastern and southwestern areas of this volcanic complex coincides with the eastern and southern flanks of this body (Ancochea et al. 1996).

In the shallower sections of the model, where the Central and North volcanic complexes are overlapped, another smaller high-density structure appears (Fig. 9). Although of minor importance, in this zone the Basal Complex is exposed to the surface (Fig. 3). Hence, it is clear that the deeper sections of the model show the connection between this small body and the deep structure of the island.

With respect to the NVC, another main positive density contrast body appears on the northwestern coast. It emerges from the deepest part of the model and rises up to the shallowest zones (Fig. 9). Therefore, it is likely be related to the building process of the island. This kind of deep structure agrees with an outcrop of BC on the surface also existing in this zone. This significant body appears to have a regular geometry at depth, but is more irregular in shallower sections where it presents a toroidal shape. This occurs only in a zone where several constructive episodes have taken place (Figs. 3, 9). It is also remarkable that this structure has a larger offshore prolongation than the other high-density bodies.

However, we must consider that, in the NVC, the OBS and BC are partially overlain by younger volcanism (Recent Series) and sediments. This explains the existence of bodies with low density in the middle north section of the shallower levels of the model (above $z = -4{,}000$ m), which are due to the presence of scattered pyroclastic cones associated with this volcanism.

With respect to the SVC, all sections of the model show a high-density body, occupying almost the whole of the Jandía Peninsula, that is independent of the other important high-density units identified in the island (Fig. 9). The existence of this unique structure is in accordance with the formation of a peninsula exclusively by OBS materials from the successive constructive episodes, and its centre coincides with the zone where most of the dykes converge on Jandía area (Ancochea et al. 1996). This main structure of the SVC proceeds from the deepest sections detected in the model, where it appears connected with the most westerly offshore body with positive density contrast, in the periphery of the model. Bathymetry at the southwest of Jandía (Figs. 3, 9) indicates this important peripheral high-density structure corresponds to the El Banquete seamount. This seamount shows a circular shape that can be interpreted as corresponding to independent edifices but connected to the SVC by a flat and shallow (20–30 m) platform (Ancochea et al. 1996). However, in the deep sections of the model, both structures appear related. The modern-day peninsula of Jandía could be the result of several building and uplift episodes, reflected in the regular geometry of these bodies, and long periods of rest and erosion.

In El Jable, where the peninsula is joined to the rest of the island, there is a secondary high-density zone, with the same direction that Ancochea found for the main trend of dyke intrusion (Figs. 3, 9).

The most notable offshore feature north of the peninsula is the existence of low-density zones. This can be evidence of a wide depression that filled as a consequence of a slide, which also originated the Jandía escarpment. Nevertheless, nothing offshore north of the peninsula seems to indicate the existence of a large central volcano with its centre situated in this zone. Furthermore, few sections of the gravity inversion model have the radial, semicircular distribution of structures with density contrasts which would support this theory.

In a general view of the model, the alignment of these high-density buildings is clear, indicating the original position of the primitive seamounts where island formation began. While those that correspond to the SVC and CVC are found to be onshore today, the structure corresponding to NVC is detected slightly offshore. This supports the idea of Ancochea et al. (1996) that the NVC was centred west and onshore.

In a broad way, the bodies with negative density contrasts are not important in the island, although they surround the coast in a very remarkable form. These bodies, bordering the island in the model, must be interpreted with caution because of their emplacement. Nevertheless, the low-density zone in the eastern border of the deeper sections of the model, which seems to come from the transition zone between Fuerteventura and Africa, can be associated with the general tectonics of the island produced by the uplift and construction of the edifices, forming the volcanic complexes in Fuerteventura.

Summary and conclusions

We have developed a genetic algorithm to solve the gravity inversion problem. According to several fixed density contrasts, this algorithm determines the geometry of the sources of the anomaly gravity field in a 3-D context. This method has been tested by a synthetic example, which has been efficiently modelled from gravity data. The results show a correct identification of the sources of the gravity field and a good fit to the observed data.

The application of the genetic algorithm to the dataset observed on the island of Fuerteventura show the applicability of the methodology in real cases. With this aim, we have compiled and analysed several gravity datasets. Thus, we have obtained a Bouguer gravity anomaly map for the island of Fuerteventura and the surrounding area. By means of our genetic algorithm, we have identified crustal structures related to the origin and evolution of the island, modelling several sources of the gravity field connected with the three volcanic complexes recognized on Fuerteventura. The Basal complex is judged the most important formation, and it appears from deepest sections to the shallowest ones of the calculated crustal model. Moreover, the structural

trends are identified and the latest volcanism (Recent Series) occurring in the island is found to be related with zones of low density contrasts.

The gravity study made in Fuerteventura has given rise to identify crustal structures, which are coherent with other geophysical and geological studies. This fact shows that the proposed method to invert gravity data functions efficiently and provides new information about the sources of the gravity field.

Acknowledgements This study was funded by the Spanish Projects: REN2001-2271/RIES (Plan Nacional I+D, MCYT), REN2002-00544/RIES (Plan Nacional I+D, MCYT). One of the authors (J. Arnoso) is supported by the program I3Pof the European Social Fund.

References

Abdel Monem A, Watkins ND, Gats PW (1971) Potasium-argon ages, volcanic stratigraphy, and geomagnetic polarity history of the Canary islands: Lanzarote, Fuerteventura, Gran Canaria and La Gomera. Am J Sci 271:490–521

Al-Chalabi M (1971) Some studies relating to nonuniqueness in gravity and magnetic inverse problems. Geophysics 36(5):835–855

Ancochea E, Brändle JL, Cubas CR, Hernán F, Huertas MJ (1996) Volcanic complexes in the eastern ridge of the Canary Islands: The Miocene activity of the island of Fuerteventura. J Volcanol Geotherm Res 70:183–204

Araña V, Camacho AG, Garcia A, Montesinos FG, Blanco I, Vieira R, Felpeto A (2000) Internal structure of Tenerife (Canary islands) based on gravity, aeromagnetic and volcanological data. J Volcanol Geotherm Res 103(4):43–64

Arnoso J (1996) Modelización y evaluación de efectos indirectos sobre las mareas terrestres en el área de las Islas Canarias. Ph D Thesis, Univ Complutense of Madrid, pp 1–175

Baker JE (1987) Reducing bias and inefficiency in the selection algorithm. In: Grefenstette JJ (ed) Proceedings of second international conference on genetic algorithms. Lawrence Erlbaum Associates, Hillsdales, pp 14–21

Banda E, Dañobeitia JJ, Suriñach E, Ansorge J (1981) Features of crustal structure under the Canary Islands. Earth Planet Sci Lett 55:11–24

Barbosa VCF, Silva JBC, Medeiros WE (1997) Gravity inversion of basements relief using approximate equality constraints on depths. Geophysics 62:1745–1757

Beltrao JF, Silva JBC, Costa JC (1991) Robust polynomial fitting method for regional gravity estimation. Geophysics 56(1):80–89

Billings S, Kennett B, Sambridge M (1994) Hypocentre location: genetic algorithms incorporating problem specific information. Geophys J Int 118:693–706

Blickle T, Thiele L (1995) A comparison of selection schemes used in genetic algorithms. TIK-Report, 11, 2nd edn. Computer Engineering and Communication Networks Lab (TIK), Zurich, pp 1–65

Boschetti F, Denith MC, List RD (1996) Inversion of seismic refraction data using genetic algorithms. Geophysics 61:1715–1727

Boschetti F, Denith MC, List RD (1997) Inversion of potential field data by genetic algorithms. Geophys Prospect 45:461–478

Bosshard E, MacFarlane DJ (1970) Crustal structure of the W Canary Islands from seismic refraction and gravity data. J Geophys Res 75:4901–4918

Camacho AG, Montesinos FG, Vieira, R (1997) A three-dimensional gravity inversion applied to S Miguel island (Azores). J Geophys Res 102(B4):7717–7730

Camacho AG, Montesinos FG, Vieira R (2000) Gravity inversion by means of growing bodies. Geophysics 65(1):95–101

Camacho AG, Montesinos FG, Vieira R, Arnoso J (2001) Modelling of crustal anomalies of Lanzarote (Canary Islands) in light of gravity data. Geophys J Int 147:1–22

Canales JP, Ito G, Detrick RS, Siton J (2002) Cristal thickness along the western Galápagos Spreading centerand the compesation of the Galápagos hotspot swell. Earth Planet Sci. Lett 203:311–327

Cantagrel JM, Fúster JM, Pin C, Renaud U, Ibarrola E (1993) Age Miocène inférieur des carbonatites de Fuerteventura (23 Ma: U–Pb zircon) et le magmatisme précoce d'une île océanique (îles Canary Islands). CR Acad Sci Paris 316:1147–1153

Carlson AL, Raskin GS (1984) Density of oceanic crust. Nature 311:555–558

Carracedo JC (1996) A simple model for the genesis of large gravitational landslide hazards in the Canary Islands. In: McGuire WJ, Jones AP, Neuberg J (eds) Volcano Instability on the Earth and Terrestrial Planets. Geol Soc London, Spec Publ 110, pp 125–135

Chandrasekhar DV, Mishra DC, Poornachandra Rao GVS, Mallikharjuna Rao J (2002) Gravity and magnetic signatures of volcanic plugs related to Deccan volcanism in Saurashtra, India and their physical and geochemical properties. Earth Planet Sci Lett 201:277–292

Chu PCH (1997) A genetic algorithm approach for combinatorial optimisation problems. PhD Thesis. The Management school, Imperial College of Science, Technology and Medicine, Londres

Coello J, Cantagrel JM, Hernán F, Fúster JM, Ibarrola E, Ancochea E, Casquet C, Jamond C, Díaz de Téran JR, Cendrero A (1992) Evolution of the eastern volcanic ridge of the Canary Islands based on new K-Ar data. J Volcanol Geotherm Res 53:251–274

Cordell L (1973) Gravity analysis using an exponencial density-depth function-San Jacinto Graben, California. Geophysics 38(4):684–690

Cubas CR, Hernan F, Ancochea E, Brandle JL (1992) El edificio sur (Jandía) de la serie I de Fuerteventura: rasgos generales. Geogaceta 11:79–81

Dañobeitia JJ (1980) Interpretación de la estructura de la corteza en el archipiélago Canario a partir de perfiles sísmicos de profundidad. Ph Thesis, Universidad Complutense de Madrid, pp1–91

Dañobeitia JJ, Canales JP (1994) An estimation of the elastic thickness of the lithosphere in the Canary Archipelago using admittance function. Geophys Res Lett 21(24):2649–2652

Dañobeitia JJ, Canales JP (2000) Magmatic underplating in the Canary Archipelago. J Volcanol Geotherm Res 103:27–41

Dañobeitia JJ, Collette BJ (1989) Estudio mediante sísmica de reflexión de un grupo de estructuras submarinas situadas al Norte y Sur del archipiélago Canario. Acta Geol Hisp 24:147–163

Davis L (1991) Handbook of genetic algorithms. Van Nostrand Reinhold, pp 1–385

De Jong KA (1975) An analysis of the behaviour of a class of genetic adaptive systems. PhD Thesis, Dept Computer and Communication Sciences, Univ de Michigan, Ann Arbor

Farquharson CG, Oldenburg DW (2004) A comparison of automatic techniques for estimating the regularization parameter in non-linear inverse problems. Geophys J Int 156:411–425

Feraud G (1981) Datations des reseaux de dykes et de roches volcaniques sous-marines par les méthodes K–Ar et ^{40} Ar–^{39} Ar Utilisation des dykes comme marqueurs de paleocontraintes, PhD Tesis, Univ Nice, pp 1–146

Folger DW, McCullough JR, Irwin BJ, Dodd JE, Strahle WJ, Polloni CF, Bouse RM (1990) Map showing free-air gravity anomalies around the Canary Islands, Spain. Miscellaneous Field Studies Map, MF-2098-B, p (1 sheet). US Geol Surv, United States

Goldberg DE (1989) Genetic algorithms in search, optimization and machine learning. Addison, Wesley, Reading, pp 1–412

Grefenstette JJ (1986) Optimization of control parameter for genetic algorithms. IEEE Transact Syst Man Cybernet SMC-16 1:122–128

Kauahikaua J, Hildenbrand T, Webring M (2000) Deep magmatic structures of Hawaiian volcanoes, imaged by three-dimensional gravity models. Geology 28 (10):883–886

Krastel S, Schmincke HU, Jacobs CL, Rihm R, Le Bas TP, Alibés B (2001) Submarine landslides around the Canary Islands. J Geophys Res 106(B3):3977–3997

MacFarlane DJ, Ridley WI (1969) An interpretation of gravity data for Lanzarote, Canary Islands. Earth Planet Sci Lett 6:431–436

Malengreau B, Lenat JF, Froger JL, (1999) Structure of Reunion Island (Indian Ocean) inferred from the interpretation of gravity anomalies. J Volcanol Geotherm Res 88:131–146

Medeiros WE, Silva JBC (1996) Geophysical inversion using approximate equality constraints. Geophysics 61(2):1678–1688

Michalewicz Z (1994) Genetic algorithms + Data structures = Evolution programs, Springer, Berlin, 2nd extended edition. pp 1–340

Montesinos FG (2002) In: Cabildo de Fuerteventura (ed) Inversión gravimétrica 3D por técnicas de evolución, Aplicación a la isla de Fuerteventura, PhD Thesis (1999), Universidad Comlutense de Madrid, pp 1–209

Montesinos FG, Camacho AG, Nunes JC, Sousa C, Vieira R (2003) A 3-D gravity model for a volcanic crater in Terceira Island (Azores). Geophys J Inter 154:393–406

Montesinos FG, Arnoso J, Benavent M, Vieira R (2004) Estudio gravimétrico en El Hierro (I. Canarias): Resultados preliminares. Proceedings of IV Asamblea Hispano-Portuguesa de Geodesia y Geofísica, pp 359–360

National Geophysical Data Center (NGDC) (1988) Data announcement 88-MGG-02, Digital relief of the surface of the Earth. NOAA, National Geophysical Data Center, Boulder

Nettleton LL (1939) Determination of density for reduction of gravimeter observations. Geophysics 4:176–183

Pick M, Pícha J, Vyskočil, V (1973) Theory of the Earth's gravity field. Elsevier, Amsterdam, pp 1–438

Ranero CR, Torne M, Banda E (1995) Gravity and multichannel seismic reflection constraints on the lithospheric structure of the Canary swell. Mar Geophys Res 17:519–534

Reeves CR (1993) Using genetic algorithms with small populations. In: Proceedings of 5th International conference on genetic algorithms. University of Illinois at Urbana-Champaign. Morgan Kaufmann Publishers, pp 92–99

René RM (1986) Gravity inversion using open, reject, and "shape of-anomaly" fill criteria. Geophysics 51:988–994

Roest WR, Dañobeitia JJ, Verhoef J, Collette BJ (1992) Magnetic anomalies in the Canary Basin and the Mesozoic evolution of the Central North Atlantic. Mar Geophys Res 14:1–24

Rothman DH (1985) Nonlinear inversion, statistical mechanics, and residual statics estimation. Geophysics 50:2784–2796

Rousset D, Lesquer A, Bonneville A, Lenat JF (1989) Complete gravity study of Piton de la Founaise volcano, Réunion Island. J Volcanol Geotherm Res 36:37–52

Rymer H, Brown CG (1986) Gravity field and the interpretation of volcanisc structures: geological discrimination and temporal evolution. J Volcanol Geotherm Res 27:229–254

Scales JA, Tenorio L (2001) Tutorial Prior information and uncertainty in inverse problem. Geophysics 66(2):389–397

Schmincke HU (1982) Volcanic and chemical evolution of the Canary Islands. In: Von Rad U, Hinz K, Sarnthein M, Seibold E (eds) Geology of the Northwest African Continental Margin. Springer, Berlin, Heidelberg New York, pp 273–301

Schwarz KP (1979) Geodetic improperly posed problems and their regularization. Bolletino di Geodesia e Scienze Affini 3:389–416

Sen M, Stoffa PL (1995) Global optimization methods in geophysical inversion, Advances in exploration geophysics, 4th ed. Elsevier, Amsterdam, pp 1–281

Silva JBC, Medeiros WE, Barbosa VCF (2001) Potential-field inversion: choosing the appropriate technique to solve a geologic problem. Geophysics 66(2):511–520

Socías I, Mezcua J (1996) Levantamiento aeromagnético del archipiélago canario. Instituto Geográfico Nacional Madrid Publ Técnica 35:1–28

Spears WM, De Jong KA (1991) On the virtues of parameterized uniform crossover. In: Belew R, Booker L (eds) Proceedings of the fourth international conference on genetic algorithm, La Jolla, Morgan Kaufmann, San Mateo, pp 230–236

Stillman CJ (1999) Giant Miocene landslides and the evolution of Fuerteventura, Canary Islands. J Volcanol Geotherm Res 94:89–104

Stillman CJ, Fuster J, Bennel-Baker M, Muñoz M, Smewing J, Sagredo J (1975) Basal complex of Fuerteventura is an oceanic intrusive complex with rift-system affinities. Nature 257:469–471

Tarantola A (1987) The inverse problem theory: Methods for data fitting and model parameter estimation. Elsevier Science Publ Co, Amsterdam, pp 1–613

Zucca JJ, Hill DP, Kovach RL (1982) Crustal structure of Muna Loa Volcano, Hawaii from seismic refraction and gravity data. Bull Seismol Soc Am 72:1535–1550